Chem Catalysis

CellPress

Article

Defect engineering over anisotropic brookite toward substrate-specific photo-oxidation of alcohols

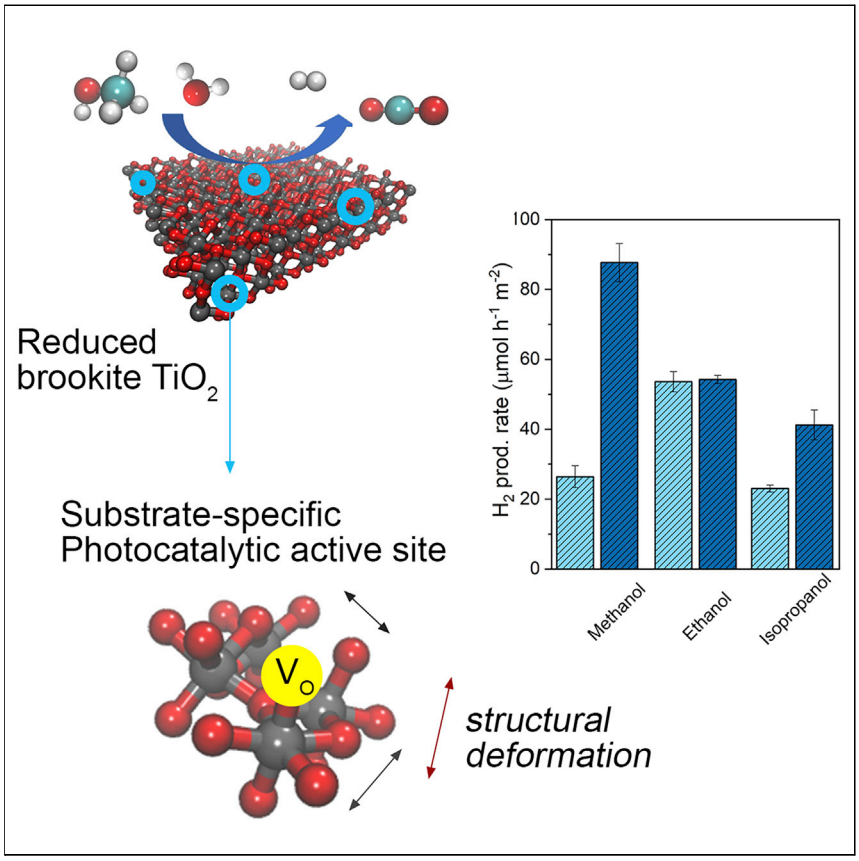

Design strategies for enhancing the photocatalytic activity leverage the tuning of the visible light response, the exposed crystal facets, and the nanocrystal shape. The formation of engineered defects in TiO_2 brookite nanorods induces active sites that enable a substrate-specific reactivity toward the photo-oxidation of alcohols and a concomitant enhanced photocatalytic hydrogen evolution. This work introduces a new design paradigm based on the electronic interactions between the photocatalyst's atomic sites and the reacting substrates.

S. M. Hossein Hejazi, Mahdi Shahrezaei, Piotr Błoński, ..., Michal Otyepka, Alberto Naldoni, Paolo Fornasiero

alberto.naldoni@upol.cz (A.N.)
pfornasiero@units.it (P.F.)

Highlights

Brookite TiO_2 nanorods with lattice strain and oxygen vacancies are synthesized

Defects in the reduced brookite enhance photocatalytic methanol oxidation rates

Reduced brookite shows a substrate specificity in the photoreforming of alcohols

The photocatalytic active site is determined by *in situ* advanced characterizations

Hejazi et al., Chem Catalysis *2*, 1177–1190
May 19, 2022
https://doi.org/10.1016/j.checat.2022.03.015

Chem Catalysis

CellPress

Article

Defect engineering over anisotropic brookite toward substrate-specific photo-oxidation of alcohols

S. M. Hossein Hejazi,[1] Mahdi Shahrezaei,[1,2] Piotr Błoński,[1] Mattia Allieta,[3] Polina M. Sheverdyaeva,[4] Paolo Moras,[4] Zdeněk Bad̆ura,[1] Sergii Kalytchuk,[1] Elmira Mohammadi,[1] Radek Zbořil,[1,5] Štěpán Kment,[1,5] Michal Otyepka,[1,6] Alberto Naldoni,[1,*] and Paolo Fornasiero[7,8,9,*]

SUMMARY

Generally adopted strategies for enhancing the photocatalytic activity are aimed at tuning the visible light response, the exposed crystal facets, and the nanocrystal shape. Here, we present a different approach for designing efficient photocatalysts displaying a substrate-specific reactivity upon defect engineering. The platinized, defective anisotropic brookite TiO_2 photocatalysts are tested for alcohol photoreforming showing up to an 11-fold increase in methanol oxidation rate, compared with the pristine one, while presenting much lower ethanol or isopropanol specific oxidation rates. We demonstrate that the substrate-specific alcohol oxidation and hydrogen evolution reactions are tightly related, and when the former is increased, the latter is boosted. The reduced anisotropic brookite shows up to 18-fold higher specific photoactivity with respect to anatase and brookite with isotropic nanocrystals. Advanced *in situ* characterizations and theoretical investigations reveal that controlled engineering over oxygen vacancies and lattice strain produces large electron polarons hosting the substrate-specific active sites for alcohol photo-oxidation.

INTRODUCTION

The visionary idea of a world powered by solar light proposed by G. Ciamician more than a century ago[1] has become a reality, proving that complex organic synthesis[2,3] and production of solar fuels like hydrogen[4–6] and ammonia[7,8] can be performed more and more efficiently. However, these intrinsically sustainable processes, before becoming industrially competitive with existing polluting technologies, need further material design, fine-tuning of light-absorption properties, charge carrier management, and surface engineering.[9] Over the past decades, photocatalysis for direct conversion of solar energy into molecular fuels has been focused on designing efficient photocatalysts by improving their fundamental properties. The visible light photoactivity can be enhanced by engineering heterojunction, introducing lattice defects into wide bandgap materials like TiO_2,[10–12] or choosing semiconductors having small bandgap energy (e.g., Cu_2O, $ZnIn_2S_4$, and C_3N_4) and suitable bands position straddling the molecular redox levels of the investigated chemical reaction.[2,13–15] The use of inorganic nanocrystals with well-defined morphology, determined crystal facets, or dimensional anisotropy have been also demonstrated to be beneficial for the charge carrier separation.[16–18] The kinetic competition between charge recombination and surface catalysis is often overcome

The bigger picture

Photocatalytic hydrogen production coupled to the controlled oxidation of biomass under ambient conditions is one of the most promising technologies for the development of the sustainable chemical industry. Despite that many efficient photocatalysts for hydrogen evolution have been discovered, the exploration of the photo-oxidation reaction and its relation with the reductive cycle, i.e., the hydrogen evolution, remain elusive. This work engineered the photocatalytic active sites for enhancing methanol oxidation by introducing sub-surface oxygen vacancies and lattice strain in reduced brookite TiO_2 nanorods, which are employed in the hydrogen evolution from alcohol photoreforming. It also shows that the reductive and oxidative photocatalytic cycle rates are tightly connected and that the engineered defects induced a rich substrate-specific reactivity depending on the alcohol employed for the photoreforming reaction.

by the addition of proper metallic co-catalysts.[19] This playground has stimulated the exploration of countless options to prepare, mix, and engineer semiconductor photocatalysts with enhanced opto-electronic properties with the aim of more efficiently driving benchmark photocatalytic reactions such as hydrogen evolution from water splitting and photoreforming of biomass. However, the majority of these studies involve monitoring the products of the reductive cycle, i.e., the evolved hydrogen, while not analyzing the oxidation products.[20–22] When sacrificial biomass substrates are employed, i.e., alcohol photoreforming, analyzing the oxidation pathway and reactivity becomes especially important not only because they provide a kinetic gain, and therefore an improved hydrogen evolution compared with the case of water oxidation, but also because the oxidized sacrificial agents often participate in hydrogen evolution, thus directly regulating its kinetics.[20,23] Furthermore, controlling the oxidation process of sacrificial biomass is particularly relevant since it can lead to its partial oxidation and the synthesis of added value products, such as 2,5-furandicarboxylic acid (bioderived polymer that may substitute PET) and diesel fuel precursors.[3,24,25]

We developed an approach to designing anisotropic defective brookite TiO_2 nanocrystals that upon high-temperature reduction treatment expose the precise defect site with substrate-specific photo-reactivity for methanol oxidation, compared with higher alcohols such as ethanol and isopropanol (Figure 1A). We show that the reaction rates for the photocatalytic alcohol oxidation and the parallel hydrogen evolution reaction are tightly connected and that optimization of the methanol oxidation leads to an increased production of hydrogen. Although the introduction of point defects and structural deformation results in enhanced visible light absorption and reduced charge carrier lifetime, we show that the selective affinity toward methanol oxidation of reduced brookite is the main parameter enabling a higher apparent quantum yield (AQY) for hydrogen evolution. Using a set of *in situ* characterization aided by density functional theory (DFT) calculations, we demonstrate that the substrate-specific activity is regulated by catalytic sites including sub-surface oxygen vacancies within a locally strained lattice environment that generate shallow hole traps responsible for boosting the first steps of methanol photo-oxidation. These photo-oxidation sites are crucial for the enhanced substrate-specific photoreforming activity of reduced brookite, and they form preferentially within anisotropic nanocrystals, which show 18-times higher specific hydrogen evolution rate, compared with isotropic ones, where defect sites with different energy are formed.

RESULTS AND DISCUSSION

Synthesis and characterization of brookite nanorods

To engineer the photocatalytic sites for alcohol photoreforming at the atomic level, we selected brookite TiO_2 nanorods—a promising and still poorly investigated TiO_2 polymorph—as a model material, and grew anisotropic nanostructures exposing the (210) surface on the lateral facets (Figure 1B) by hydrothermal synthesis (see supplemental experimental procedures).[26] We prepared various brookite photocatalysts reduced under an H_2 stream at different temperatures, along with reduced anatase and commercial brookite reference samples (see Table S1 and Note S1). Elemental analysis revealed that the obtained nanopowders did not contain significant quantity of non-metals coming from C, H, or N incorporation (Table S2 and Note S2). Reduction of pristine brookite TiO_2 nanorods under pure hydrogen stream at 700°C for 1 h created defective nanocrystals showing remarkable changes in their structural and electronic properties alongside giving the best photocatalytic performance. This morphology evolved from anisotropic nanostructures with well-defined shape and exposed crystal facets (Figures 1B and S1A)

[1]Czech Advanced Technology and Research Institute, Regional Centre of Advanced Technologies and Materials, Palacký University Olomouc, Křížkovského 511/8, 77900 Olomouc, Czech Republic

[2]Department of Physical Chemistry, Faculty of Science, Palacký University, 17. listopadu 1192/12, 779 00 Olomouc, Czech Republic

[3]Ronin Institute Montclair, Montclair, NJ 07043, USA

[4]Istituto di Struttura della Materia-CNR (ISM-CNR), SS 14, Km 163,5, 34149 Trieste, Italy

[5]Nanotechnology Centre, Centre of Energy and Environmental Technologies, VŠB–Technical University of Ostrava, 17. listopadu 2172/15, 70800 Ostrava-Poruba, Czech Republic

[6]IT4Innovations, VSB – Technical University of Ostrava, 17. listopadu 2172/15, 708 00 Ostrava-Poruba, Czech Republic

[7]Department of Chemical and Pharmaceutical Sciences, ICCOM-CNR Trieste Research Unit, INSTM-Trieste, University of Trieste, Via L. Giorgieri 1, 34127 Trieste, Italy

[8]Center for Energy, Environment and Transport Giacomo Ciamician - University of Trieste, Trieste, Italy

[9]Lead contact

*Correspondence: alberto.naldoni@upol.cz (A.N.), pfornasiero@units.it (P.F.)

https://doi.org/10.1016/j.checat.2022.03.015

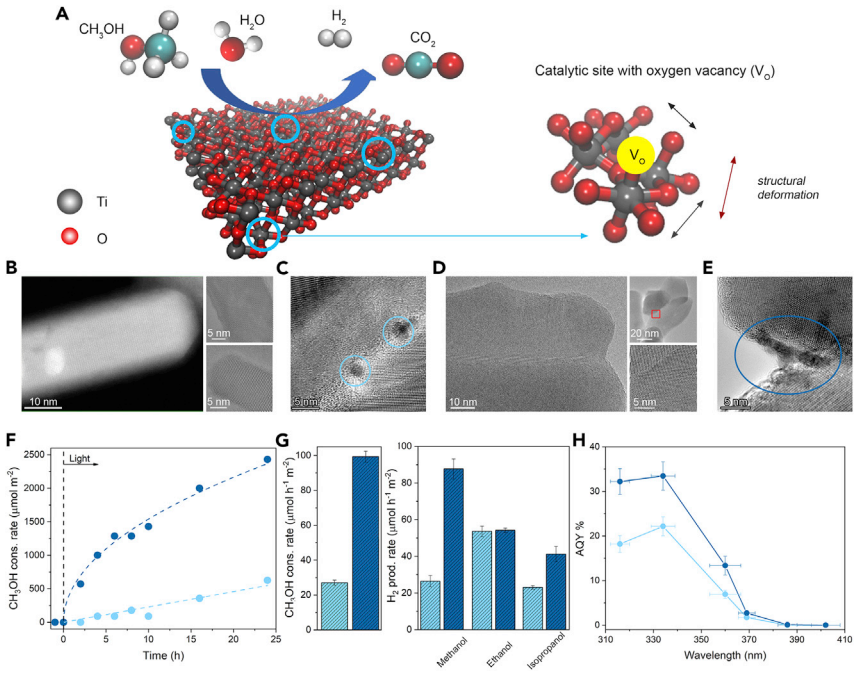

Figure 1. Morphology and photocatalytic activity

(A) Schematic representation of defect engineering in reduced brookite showing an exemplary TiO_2 surface during photocatalysis and a zoomed-in view of the catalytic site containing oxygen vacancy (V_O) and structural distortions.

(B) HAADF-STEM (left) and HRTEM (right) micrographs of a single brookite nanorod.

(C) HRTEM micrograph of isolated Pt nanoparticles deposited on pristine brookite.

(D) HRTEM of brookite nanorods reduced at 700°C.

(E) HRTEM micrograph of aggregated Pt nanostructures deposited on reduced brookite.

(F) Methanol consumption in time for pristine (sky blue) and reduced brookite (dark blue) nanorods. The points before zero time represent the methanol signal before adding the photocatalysts, while time zero was measured once the adsorption/desorption equilibrium in the dark was reached.

(G) Specific methanol consumption rate (left) and specific hydrogen evolution rate (right) during methanol, ethanol, and isopropanol photoreforming for pristine (sky blue) and reduced (dark blue) brookite. Measurements were performed under a simulated AM 1.5G spectrum at one-sun intensity for 24 h using a 1:1 vol % H_2O:alcohol mixture.

(H) AQY for hydrogen evolution from methanol photoreforming for pristine (sky blue) and reduced (dark blue) brookite. In all measurements both pristine and reduced brookite were loaded with 1 wt % Pt.

into more isotropic nanoparticles that displayed irregular shape and aggregation through twin boundaries formation (Figures 1C and S1B). Notably, anatase and brookite with isotropic crystal shapes (Figures S2 and S3 and Note S3) did not reveal any crystal reshaping upon high-temperature reduction treatment. However, they presented different color variations (Table S1), compared with those observed for the anisotropic brookite, upon increasing the temperature of the hydrogen treatment, thus suggesting a different reducibility behavior with respect to the TiO_2 polymorph and crystal shape, as confirmed by UV-vis reflectance spectroscopy, Raman spectroscopy, and photoluminescence spectroscopy mapping (see below). In order to prepare highly active photocatalysts for alcohol photoreforming, we functionalized the samples by photodepositing Pt co-catalyst nanoparticles on their surface. Inductively coupled plasma mass spectrometry (ICP-MS) analysis detected similar Pt loading on both pristine (0.98 wt%) and reduced brookite samples (0.90 wt%). High-resolution transmission electron microscopy (HRTEM) and high-angle annular dark-field scanning transmission electron microscopy (STEM-HAADF) micrographs as well as the elemental mapping showed that Pt

nanoparticles with an average diameter of 2.5 nm were homogeneously deposited on the pristine brookite nanorods (Figures 1D, S4A, S5, and S6). Surprisingly, in the case of reduced brookite nanocrystals, we detected the presence of small Pt nanoparticles with similar sizes, as well as larger Pt nanoparticle aggregates reaching 10 to 30 nm in size (Figures 1E and S7–S10). This result was confirmed by an HRTEM analysis of three different brookite batches. The larger Pt conglomerates may be less reactive than the smaller ones, thus negatively affecting the photocatalytic activity of the reduced brookite. Moreover, larger metal aggregates may screen the incoming light during photocatalysis, decreasing the light harvesting efficiency. However, as shown in the next section, in the present investigation these parameters did not reduce either one aspect or the other for reduced brookite, suggesting that for the considered reaction, the defects in TiO_2 played a more crucial role than that of Pt nanoparticles. The brookite treatment under hydrogen was accompanied by a decrease in the Brunauer–Emmett–Teller (BET)-specific surface area from 67 to 47 $m^2\ g^{-1}$ after reduction (Figure S11 and Table S3).

The temperature (reduction)-dependent structural parameters extracted by the Rietveld refinement of X-ray diffraction (XRD) patterns were in agreement with the described morphological evolution (Figures S12–S18, Tables S4–S6, and Note S4). Notably, the XRD analysis highlighted that the reduction treatment introduced an anisotropic and preferential deformation of the brookite lattice along the c-axis due to the creation of oxygen vacancies (Figure S19). Their presence was further supported by the blueshift in the main A_{1g} vibrational mode detected by Raman spectroscopy measurements (Figure S20 and Note S5) after reduction, which again pointed out a different reducing behavior dependent on the TiO_2 polymorph and shape (Raman shift is 1.3 cm^{-1} for the reduced anisotropic brookite, 7.6 cm^{-1} for the reduced isotropic anatase, and no observed shift for the reduced isotropic brookite). Having performed the bond valence sum analysis, we observed an average depletion of ~0.5% of the Ti valence for the reduced brookite—a typical feature induced by the formation of oxygen vacancies.[11,27] The moderate decrease in the Ti valence upon an H_2 treatment at high temperature is an indication of a low tendency toward defects formation in brookite nanorods. This general feature was also reflected by the color change—from white to gray—that brookite underwent after reduction at 700°C, as opposed to the more reducible anatase phase that assumed a darker color already at lower temperatures (Table S1). The reduced brookite nanorods showed an optical bandgap energy of ~3.38 eV, this making no significant difference from the value retrieved for the as-synthesized sample (Figure S21 and Table S7). The same results were observed for both the isotropic brookite and anatase samples (Figures S22, S23, Tables S8, and S9). Further analysis of the absorption spectra highlighted an increased visible light absorption and an Urbach tail that ranged for the anisotropic brookite from 69 (for the as-synthesized brookite nanorods) to 115 meV (for nanorods reduced at 700°C). For the isotropic anatase, the Urbach tail increased from 115 (for the as-synthesized anatase nanoparticles) to 205 mV (for anatase reduced at 500°C). This supports the scenario of a phase- and shape-dependent increase in the population of oxygen vacancies after the reduction treatment (see Note S6).

Alcohol photoreforming with reduced brookite

The photocatalytic activity of the platinized brookite nanorods was tested for methanol photoreforming under a simulated AM 1.5G spectrum at one-sun intensity producing H_2 and oxidation products. As previously reported by other groups, the increased photocatalytic activity of reduced TiO_2 nanomaterials could be ascribed to the co-catalyst role in H_2 evolution played by oxygen vacancies.[12,28] In contrast, in order to use the oxygen vacancies as catalytic sites in the photocatalytic oxidation

reaction, we photodeposited Pt nanoparticles over the optimized photocatalysts. Following this procedure, H_2 generation occurred on the Pt surface as the photogenerated electrons were separated and stabilized into the Pt nanoparticles by the Schottky barrier formation at the Pt–TiO_2 interface, while photo-oxidation occurred on the TiO_2 surface.[19,29]

In contrast to common practice, where only an H_2 production rate is detected, we designed specific experiments to follow the kinetics of methanol photo-oxidation using a solution including deuterated methanol (i.e., CD_3OD) and a small aliquot of methanol (i.e., CH_3OH), whose corresponding consumption was followed by an ^{1}H-nuclear magnetic resonance (^{1}H-NMR) analysis of the liquid phase (Figure S24 and Note S7). Table S10 reports the NMR signal integration of CH_3OH relative to the adopted internal standard (DMSO), which highlights no significant difference between the blank measurement containing no photocatalyst and the one at time zero, i.e., after 30 min of adsorption/desorption equilibrium in the dark in the presence of the photocatalysts. From these data it is clear that the methanol adsorption in the dark did not affect the photocatalytic performance of the investigated photocatalysts. Figure 1F shows the amount of methanol oxidized over 24 h of illumination illustrating the remarkable oxidation activity of the reduced brookite over the pristine material. The corresponding specific methanol consumption rates, computed by using the BET surface area of each sample, for the platinized brookite nanorod samples (Figure 1G, left) evidenced that the pristine brookite drove the photo-oxidation reaction with a specific rate of 27 μmol h^{-1} m^{-2}, whereas for the reduced one, it was 99 μmol h^{-1} m^{-2}. We obtained the photoactivity values by considering methanol consumption after 24 h of reaction, which resulted in a 3.7-fold enhancement in favor of the reduced brookite. Notably, if we consider kinetic data after 5 h (Figure 1F), the reduced brookite performed methanol photo-oxidation up to 11 times faster than the pristine sample. This suggests on the one hand that, in the early stage of reaction, methanol was oxidized faster until the available surface reaction sites were fully occupied and a steady state was reached, which ensured a higher methanol consumption rate even after 24 h of reaction, as evidenced by the divergence of the reaction kinetics curves (Figure 1F). On the other hand, this behavior can be due to a partial aggregation of the colloidal photocatalysts after several hours of irradiation (see dynamic light scattering measurements in Figure S25), thus producing a reduced available surface for the methanol oxidation reaction to occur.

The amount of evolved hydrogen determined by gas chromatography analysis followed a linear increase with time (Figure S26) for both the pristine and the reduced brookite, corresponding to optimized specific H_2 production rates of 26 and 88 μmol h^{-1} m^{-2}, respectively, with reduced brookite that evolved H_2 3.4 times faster (Figure 1G, right). The reduced brookite showed a 13% decrease activity after five photocatalytic runs (Figure S27). Notably, the activity decrease appeared almost constant after each recycling test, thus suggesting that it can be due to the loss of catalyst during the tests, which can happen during the centrifugation/re-suspension of the photocatalyst and/or can be due to the loss of material attaching onto the reactor walls. Another aspect that can produce this slight decrease in activity is the increased hydrodynamic diameter of the brookite nanocrystals in suspension, as revealed by dynamic light scattering measurements after 24 h of illumination (Figure S25). Moreover, two more aspects may produce the observed photocatalytic activity decrease after several recycling cycles. On the one hand, the catalyst surface may be partially passivated by the presence of reaction intermediates, as we did not wash the catalyst before subsequent tests. On the other hand, a partial modification of the population of defects (as evidenced by the resonant photoemission valence band measurements on B700 after catalysis; see photoemission

spectroscopy section in the supplemental information) may induce a partial reactivity change. Interestingly, the H_2 production rates followed a reactivity trend closely resembling the one observed for the methanol photo-oxidation activity, which suggests that hydrogen production is strictly regulated by the alcohol oxidation and it can be used as reporter figure of merit for tracking the reactivity of the pristine and the reduced brookite for alcohol photo-oxidation. Following this principle, we tested our platinized samples for the photoreforming of ethanol and isopropanol and discovered that the reactivity of the reduced brookite was markedly more pronounced and substrate-specific toward methanol in comparison with the other tested alcohols (Figure 1G, right). In the case of ethanol photoreforming, both reduced and pristine anisotropic brookites showed a specific H_2 production rate of 54 $\mu mol\ h^{-1}\ m^{-2}$, suggesting that they have a similar affinity toward its photo-oxidation. On the other hand, in the case of isopropanol photoreforming, the reduced anisotropic brookite presented a 1.7-fold higher specific H_2 production rate (41 $\mu mol\ h^{-1}\ m^{-2}$) when compared with the pristine sample, denoting a higher photo-oxidation ability, yet still much lower than that shown for methanol. From the photocatalytic tests using the reference materials (Figure S28), the reduced commercial platinized brookite presented a higher reactivity toward methanol than that for the other alcohols, although showing a lower degree of specificity and reactivity if compared with the brookite nanorods (Figure 1G). This may be due to their identical crystalline phase, which implies a similar mechanism of defect formation (and reactivity). On the other hand, the platinized anatase samples showed a different pattern of reactivity, suggesting that the photocatalytic activity toward different substrates is affected by the crystalline phase, reduction treatment, and type of defects formed within the photocatalysts. This observation confirmed that the H_2 evolution activity of the reduced brookite was regulated by a substrate-specific reactivity toward alcohol photo-oxidation. Such a stark photo-reactivity toward methanol oxidation was observed for the brookite nanorods, while platinized reference samples made by reduced spherical anatase nanocrystals or reduced isotropic brookite nanoparticles displayed ~2.1 to 2.4 times higher specific photocatalytic rates (per optimized mass) in comparison with the untreated materials (from data reported in Figure S29A). Notably, the reduced brookite nanorods loaded with Pt showed a remarkably higher specific H_2 evolution rate, with respect to both the reduced anatase/Pt (16 times) and the reduced isotropic brookite/Pt (18 times), as shown in Figure S29A. This difference is reduced when considering the photocatalytic activity per optimized mass (from data reported in Figures S29B and S30), with the reduced brookite nanorods (B700/Pt) still showing more than two times the hydrogen evolution rate than that observed for the reduced anatase nanocrystals (A500/Pt).

These observations suggest that the type of produced defects/catalytic sites varies depending on the selected TiO_2 polymorph as well as on the crystal shape, which emphasizes how the exposure of different crystal facets having different interfacial energy and therefore resistance to hydrogen treatment under high temperature regulates the defect formation. This is demonstrated by the different degree of reducibility that each sample exhibited, as supported by previously discussed absorption and Raman spectroscopy measurements.

The AQY for hydrogen evolution from methanol photoreforming was measured for a pristine and a reduced platinized brookite (Figure 1H) using different monochromatic light sources. The maximum AQY was reached at 334 nm and was 33.5% for the reduced brookite and 22.2% for the pristine nanorods. These AQY values can be further increased by optimizing the methanol concentration, metal loading, metal particle size, or photoreactor design, which, however, goes beyond the scope of this study. Interestingly, despite its visible light absorption, the reduced

brookite did not show AQY in the visible region, with values of ~0.09 and 0.004% at 386 and 402 nm, respectively (AQY below the detection limit for the pristine brookite at both wavelengths). This result was further confirmed by H_2 evolution experiments under one-sun illumination applying a longpass optical filter to cut off $\lambda \geq 380$ nm, i.e., cutting optical excitation above bandgap energy did not lead to detecting any H_2 after 24 h of reaction. This result confirms that oxygen vacancies introduced upon the hydrogen treatment at high temperature, and the related optical transitions, did not produce visible light photocatalytic activity. We indeed suggest that the introduced oxygen vacancies enhanced the reactivity toward the methanol oxidation by favoring its activation, as discussed in further detail below.

In order to study in more detail the methanol photo-oxidation reaction on the reduced brookite, we analyzed the reaction products by both the gas chromatography analysis of the gas phase and the NMR analysis of the liquid phase after reaction. Carbon dioxide was the only detected reaction product. Furthermore, we investigated the hydrogen production rate from different possible intermediates of methanol oxidation (e.g., formaldehyde and formic acid) of as-synthesized and reduced brookite nanorods loaded with 1 wt% Pt. Interestingly, both samples showed similar specific photocatalytic activity in the presence of formaldehyde and formic acid, presenting significant hydrogen production rate of around 25 to 30 $\mu mol\ h^{-1}\ m^{-2}$ (Figure S31). This result is far from being trivial, as it has been reported that other TiO_2 polymorphs usually oxidize methanol to formaldehyde, thus stopping the methanol photo-oxidation after the first reaction step.[30] Moreover, it repeatedly emphasizes that a reduced brookite demonstrates a substrate-specific oxidation ability toward methanol molecules. The blank test for photolysis of formaldehyde under AM 1.5G one-sun illumination produced a very small hydrogen production rate, namely, ~85 $nmol\ h^{-1}\ m^{-2}$.

Notably, the investigated TiO_2 samples showed two order-lower alcohol photoreforming activity without Pt loading; the data on the samples reduced at different temperatures are reported in Figures S32 and S33. These data are further supported by electron spin resonance spectroscopy (EPR) investigations measured under dark and light conditions both for dried powders and in a water/methanol medium (*in situ* conditions), demonstrating the increased reactivity of brookite nanorods reduced at 700°C (Figures S34–S36). For instance, in the case of EPR spectra for dried powders of an anisotropic brookite reduced at different temperatures, the most efficient sample in methanol photoreforming was B700, which indeed gave the highest differential EPR signal (light-dark) in comparison with samples with lower activity (e.g., a pristine brookite and B500). Interestingly, the most active sample (B700) showed the weakest intensity in the EPR powder spectrum among the series (Figure S34 and Note S8). Therefore, the number of spins recorded by EPR do not directly correlate with the system reactivity and its overall efficiency in the photocatalytic process, all in agreement with previous reports.[12,31]

In situ photoluminescence spectroscopy

To understand the nature of the methanol oxidation sites, we measured excitation-dependent photoluminescence (PL) spectra at 80 K, obtaining energy-resolved two-dimensional maps of the radiative recombinations occurring in the pristine and the reduced anisotropic brookite both under inert gas atmosphere (N_2) and in the presence of methanol (Figure 2A). The PL maps in the presence of the latter (i.e., a hole scavenger) showed drastic quenching of the signal, demonstrating that the photogenerated holes trapped within the defect sites, i.e., oxygen vacancies, readily reacted with the surface adsorbed methanol molecules. Moreover, this also provided

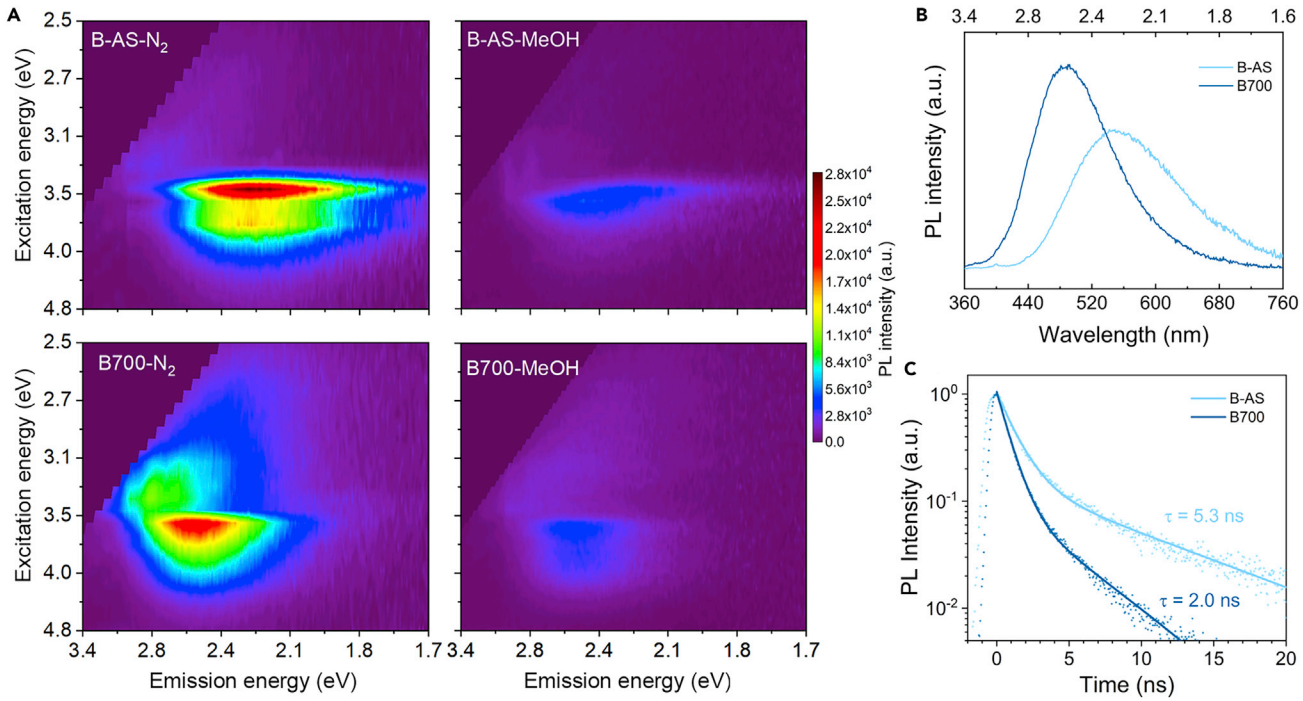

Figure 2. Energy distribution of defects-related radiative recombinations and lifetime of photogenerated charge carriers

(A) Excitation-emission color maps under N_2 and in the presence of methanol (MeOH) for pristine and reduced brookite.

(B) PL spectra of pristine (blue sky) and reduced brookite (dark blue) under excitation at 340 nm.

(C) Time-resolved PL decay curves collected at the corresponding emission maximum of pristine (blue sky) and reduced brookite (dark blue) under excitation at 372 nm.

evidence that such defect sites must be located on either the surface or sub-surface of the brookite nanocrystals, from where they can react with surface adsorbates.[32] This is supported by the synchrotron-based photoemission spectra for the Ti 2p region and valence band (see the next section for details). Comparing the two-dimensional PL maps measured under N_2 gas atmosphere for the pristine and the anisotropic brookite reduced at 500, 600, 700, and 800°C (Figures 2A and S37), we observed a clear variation in the energy position relative to the radiative recombination centers upon high-temperature treatment, eventually underlined by a subtle but significant re-organization of structural defects. Notably, the reference samples (especially the isotropic anatase, which is more reducible than the isotropic brookite) displayed a similar behavior (Figures S38, S39 and Note S9).

Focusing on the reduced anisotropic brookite, we observed a significant blue shift in the PL peak after reduction.

This is better highlighted in the PL spectra generated using a single excitation wavelength (340 nm) and by analyzing the weight of the deconvoluted components set at 2.75, 2.53, 2.27, and 2.0 eV for all the samples (Figures 2B and S40). The dominant radiative recombinations for the as-synthesized anisotropic brookite (B-AS) localize at 2.27 and 2.0 eV, while the components at higher energies are almost negligible. Notably, in the case of the reduced anisotropic brookite (B700), the component at lower energy almost vanished, while the intensity of the radiative recombinations with higher energies (2.75 and 2.53 eV) became dominant, denoting the formation of shallower hole traps upon hydrogen reduction treatment at high temperature. Furthermore, we investigated the lifetime of photogenerated charge carriers

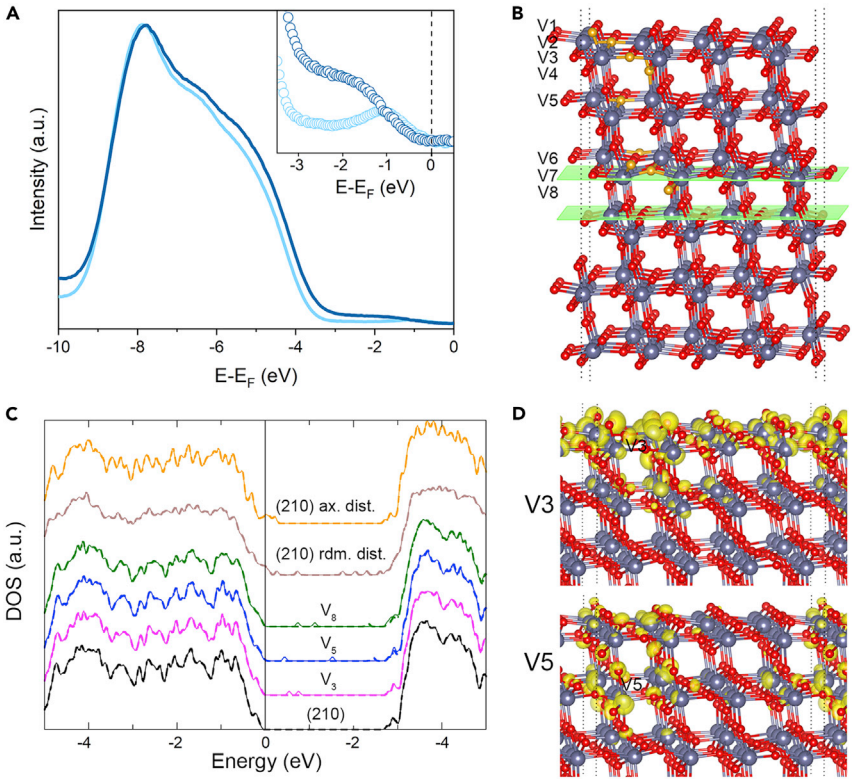

Figure 3. Experimental and theoretical determination of the electronic structure of the photocatalytic sites

(A) Synchrotron-based photoemission spectra around the VB region for the pristine (light blue) and the reduced (dark blue) brookite. Inset: zoom of the VB region around the Fermi energy.

(B) Brookite TiO_2 supercell employed for the calculations exposing the (210) surface: Ti atoms plotted in gray, O atoms in red, oxygen vacancies in orange. The middle part of the slab corresponds to the bulk region of TiO_2 enclosed by green planes, while the supercell's boundaries are marked by the dotted lines.

(C) Calculated total DOS of the ideal (210) brookite surface, of various defective brookite surfaces with an oxygen vacancy (V in the figure) placed at different locations in the lattice, two distorted brookite surfaces (rdm. and ax. indicate random and axial distortions, respectively). The energy of the VB maximum of the ideal (210) surface is taken to be zero. Spin up/down derived DOS are shown by solid/dashed lines.

(D) Excess electron density donated by introducing V3 and V5 oxygen vacancies (yellow isosurface).

measured at PL maximum by time-resolved PL spectroscopy. The charge carriers' lifetime (τ) decreased after the brookite's reduction, similarly to the other TiO_2 reference samples, from 5.3 ns to 2.0 ns (Figures 3C and S41 and Table S11), suggesting that the enhanced photocatalytic activity of the reduced anisotropic brookite is not related to the enhanced charge separation.

Synchrotron resonant photoemission spectroscopy

The investigation by conventional lab-scale X-ray photoelectron spectroscopy (XPS) analysis provided similar results for pristine and reduced TiO_2 samples (Figure S42 and Note S10). Therefore, we investigated in more detail the electronic structure of our brookite samples at the VUV-Photoemission beamline (Elettra, Trieste) by synchrotron-based photoemission spectroscopy (PES) for the Ti 2p (Figure S43), O 1s (Figure S44, see discussion in the next section), and the valence band (VB) regions. The Ti 2p spectra of both brookite samples contained two components

corresponding to the presence of Ti^{4+}, due to the coordination of Ti into the stoichiometric lattice, and Ti^{3+} species introduced by the oxygen vacancy formation near or at the TiO_2 surface. The presence of low valence Ti ions in the pristine brookite is a common observation, especially in nanocrystals obtained through hydrothermal synthesis and not subjected to a following heat treatment like in the present case. Next, by using soft X-ray photons with energy that is resonant to the Ti absorption edge, it is possible to highlight electronic states even in samples containing a low amount of defects.[33] Figure 3A shows the VB PES spectra for the pristine and the reduced anisotropic brookite. The main VB edge did not significantly shift upon reduction, while the density of states (DOS) within the bandgap showed a stark difference. The pristine brookite displayed localized mid-gap states peaking at around 1 eV below the Fermi energy. In contrast, the reduced brookite revealed an increased electron density showing an intense VB tailing. We also performed an ex situ investigation of the reduced brookite after 24 h of photocatalytic reaction B700-AR and compared the result with the spectra of the pristine brookite B-AS and the reduced brookite before reaction B700-BR (Figure S45). The post-catalytic VB spectrum shows a rigid shift of the VB minimum toward the Fermi level and a more populated DOS in the energy range from −3 to −1.5 eV (similarly to B700-BR) in comparison with the pristine material. It also features a localized state at around 1 eV below the Fermi level. The presence of these features strongly suggests that the material after photocatalysis displays similar structural/electronic features present in the reduced materials before photocatalysis, but detected with lower intensity (or to a minor extent) due to the adsorption of methoxy groups/reaction intermediates, i.e., the sample was not regenerated after reaction. The observed features detected with low intensity would not be present at all if the materials after catalysis would have been returned to the initial electronic/lattice structure. We have shown using DFT calculations that the electronic features of the reduced samples are due to both the presence of oxygen vacancies and TiO_6 octahedra deformations (different from those imparted by the oxygen vacancy site relaxation), both induced by the high-temperature treatment under hydrogen. It is not likely that the catalytic process, as supported by the presented data, eliminates the latter kind of lattice deformations. On the other hand, the populations of oxygen vacancies created in the reduced brookite are most likely located in the sub-surface, as the defects on the surface are filled/healed by the interactions with adsorbates upon exposure to air/liquids (i.e., our working conditions). This highlights that they are more protected and stable in comparison with surface defects. Therefore, all this evidence remarks that the defects created in the reduced brookite are mainly sub-surface defects, still participating to the catalytic process and that they are stable after photocatalysis, in agreement with the observed constant H_2 evolution rates.

DFT calculations of the photocatalytic sites

In order to understand the origin of the VB tailing in the electronic structure of the reduced brookite, we calculated the energy band structure using *ab initio* DFT calculations. Driven by the XRD results, we focused on the (210) surface of the brookite TiO_2 introducing two types of structural defects: (1) oxygen vacancies located at different distance from the surface (denoted by V1–V8 in Figures 3B and S46), and (2) distortion of TiO_6 octahedra (see supplemental experimental procedures) by modifying up to ± 0.1 Å either the axial or randomly chosen Ti-O distances.

The presence of oxygen vacancies introduces localized mid-gap states deriving from the hybridization of O 2p and Ti 3d orbitals (Figures 3C and S47) with their energy position that varies with respect to the defect's distance from the surface. In contrast, the primary effect of the expansion of Ti-O axial distances is to produce strong band

tailing near the VB edge (Figure 3C) entering the band gap by ~0.4 eV. When we introduced a lattice disorder by random displacements of both Ti and O atoms from their equilibrium positions, both mid-gap states and VB tailing were seen in the DOS (Figure 3C). The computational results confirmed that the DOS envelope of the reduced brookite was formed by mid-gap states and VB band tailing due to the combined effect of oxygen vacancies and lattice distortions. The location of oxygen vacancies in the real samples is represented by a statistical distribution of lattice positions. Each of such defect populations produce different DOS and their convolution, alongside the effect from lattice distortions, results in the formation of the VB tailing. Importantly, the oxygen vacancies in the reduced brookite nanorods are most likely located in the sub-surface region, as the defects on the surface are filled/healed by the interactions with adsorbates upon exposure to air/liquids (i.e., our working conditions).

We also examined the differential electron densities due to the introduction of an oxygen vacancy at two different positions in the slab, namely, surface/near-surface (V3) or sub-surface (V5) positions (Figures 3B and 3D). In both cases, the excess of charge was spread over many lattice sites and accompanied by the relaxation of the lattice atoms by up to 2% to 4% of the equilibrium Ti-O bond length, thus denoting the generation of a large electron polaron around the oxygen vacancies.

We propose that these kinds of bound states between oxygen vacancies and large electron polarons represent the substrate-specific photocatalytic active sites for methanol oxidation. The size of this photocatalytic active site and the charge distribution around it favor a high specificity toward the methanol molecule rather than to higher alcohols. The finding of Zhang and co-workers supports our results, as they recently observed a similar reactivity pattern in Cu-doped TiO_2 nanosheets, where the oxygen vacancies within a strained environment enabled strong chemisorption and activation of molecular N_2 and water, resulting in high photocatalytic NH_3 evolution under visible light irradiation.[8] Diebold and co-workers recently reported the photo-oxidation mechanism of methanol at the surface of anatase TiO_2.[34] Values obtained from DFT calculations, scanning tunneling microscopy, and temperature programmed desorption aided by XPS showed the existence of two different, more favorable pathways for activating methanol adsorbed on TiO_2. Methanol molecules are first adsorbed onto the surface Ti_{5c} atoms dissociating into methoxy groups and hydrogen atoms, which are then oxidized to formaldehyde (and eventually to formic acid and carbon dioxide) and molecular hydrogen. Methanol molecules must first dissociate into methoxy groups, and after this step, the hole transfer from TiO_2 becomes energetically favorable. Methanol can be activated via two pathways (Figure S48): (A) by reaction with dissociated H_2O forming terminal OH^- species bound to surface Ti_{5c} atoms, and (B) by reaction with activated adsorbed O_2.[34] Mechanism (A) begins with the spontaneous dissociative adsorption of water enabled by the extra charge density due to oxygen vacancies and reflected by the formation of hydroxyl ions.[34,35] Interestingly, brookite TiO_2(210) (the same crystallographic direction expressed on the lateral facets of our brookite nanorods) has the same structural building block of anatase TiO_2(101), but interatomic distances are slightly shorter and the blocks are arranged in a different way. Selloni and co-workers found that these differences significantly change the reactivity toward adsorption of water (and formic acid), making its dissociation more possible to occur on the brookite surface rather than on the anatase.[36] This may underlie the enhanced specific photocatalytic activity that we observed for the anisotropic brookite over the anatase during methanol photoreforming. This scenario is corroborated by the synchrotron PES of the O 1s region that shows a significant, 24% increase in the OH^- species adsorbed on the reduced surface in comparison with the pristine brookite. These

species may be derived from the dissociative adsorption of water, which is more favored on the reduced brookite due to the extra electrons provided by the sub-surface oxygen vacancies.[32] Mechanism (B) is less probable, as our experiments are performed in the absence of oxygen (under Ar atmosphere). However, it should be noted that some traces of peroxide species were detected by EPR,[12,37] suggesting that mechanism (B) may occur even at a lower extent than mechanism (A). This could also point to a faster decomposition of hydrogen peroxide to water and bridging oxygen dimer (step (iii) → (iv) in mechanism B) in the most photoactive sample (B700) after illumination. Finally, besides the pure (A) and (B) mechanisms, an intermediate case can be also considered, in which the OH^- formation results from the reaction of coadsorbed O_2 and H_2O.[38]

Conclusions

In summary, we demonstrated the concept of enhancing the photocatalytic activity during alcohol photoreforming by engineering the defect sites in an anisotropic platinized brookite in a way that enables substrate-specific oxidation photoactivity. Synchrotron photoemission spectroscopy and *in situ* photoluminescence investigations aided by DFT calculations showed that creating a low amount of defects (i.e., oxygen vacancies) in well-defined lattice positions produces a kind of bound state between oxygen vacancies and large electron polarons hosting the photocatalytic active sites, which act as shallow hole traps during alcohol photoreforming. Our results also demonstrate that the nature of the produced defects/photocatalytic sites varies with respect to the selected TiO_2 polymorph and on its crystal shape. This work highlights the value of analyzing the reaction products of both the reductive and the oxidative pathways during photocatalytic reactions alongside opening new avenues for substrate-selective photocatalytic biomass conversion through the atomic design of the active sites.

EXPERIMENTAL PROCEDURES

Resource availability

Lead contact

Further information and requests for resources and reagents should be directed to and will be fulfilled by the lead contact, Paolo Fornasiero (pfornasiero@units.it).

Materials availability

All materials generated in this study are available from the lead contact without restriction.

Data and code availability

All data needed to support the conclusions of this manuscript are included in the main text or supplemental information.

SUPPLEMENTAL INFORMATION

Supplemental information can be found online at https://doi.org/10.1016/j.checat.2022.03.015.

ACKNOWLEDGMENTS

A.N. and R.Z. gratefully acknowledge the support of the Czech Science Foundation (GACR) through the projects no. 20-17636S and 19-27454X. The authors gratefully acknowledge the support by the Operational Programme Research, Development and Education - European Regional Development Fund, project no. CZ.02.1.01/0.0/0.0/15_003/0000416 of the Ministry of Education, Youth and Sports of the Czech Republic. P.F. acknowledges financial support from the European Community

(projects H2020 – RIA-CE-NMBP-25 Program [grant no. 862030] and H2020-LC-SC3-2019-NZE-RES-CC [grant n 884444]), INSTM consortium, and ICCOM-CNR. P.M.S. and P.M. gratefully acknowledge financial support through the project EUROFEL-ROADMAP ESFRI. The authors gratefully acknowledged G. Zoppellaro and O. Tomanec for EPR discussion and TEM measurements, respectively.

AUTHOR CONTRIBUTIONS

Conceptualization, P.F. and A.N.; methodology, S.M.H.H., M.A., E.M., and P.B.; investigation, S.M.H.H., M.S., P.M.S., P.M., Z.B., S.K., E.M., and P.B.; visualization, S.M.H.H., P.B., and A.N.; funding acquisition, R.Z., S.K., M.O., P.F., and A.N.; project administration, A.N.; supervision, P.F. and A.N.; writing – original draft, S.M.H.H. and A.N.; writing – review & editing, S.M.H.H., M.A., P.M., P.B., R.Z., M.O., P.F., and A.N.

DECLARATION OF INTERESTS

The authors declare no competing interests.

Received: October 15, 2021
Revised: February 7, 2022
Accepted: March 21, 2022
Published: April 13, 2022

REFERENCES

1. Ciamician, G. (1912). The photochemistry of the future. Science *36*, 385–394.
2. Ghosh, I., Khamrai, J., Savateev, A., Shlapakov, N., Antonietti, M., and König, B. (2019). Organic semiconductor photocatalyst can bifunctionalize arenes and heteroarenes. Science *365*, 360–366.
3. Luo, N., Montini, T., Zhang, J., Fornasiero, P., Fonda, E., Hou, T., Nie, W., Lu, J., Liu, J., Heggen, M., et al. (2019). Visible-light-driven coproduction of diesel precursors and hydrogen from lignocellulose-derived methylfurans. Nat. Energy *4*, 575–584.
4. Wang, Q., Hisatomi, T., Jia, Q., Tokudome, H., Zhong, M., Wang, C., Pan, Z., Takata, T., Nakabayashi, M., Shibata, N., et al. (2016). Scalable water splitting on particulate photocatalyst sheets with a solar-to-hydrogen energy conversion efficiency exceeding 1%. Nat. Mater. *15*, 611–615.
5. Kosco, J., Bidwell, M., Cha, H., Martin, T., Howells, C.T., Sachs, M., Anjum, D.H., Gonzalez Lopez, S., Zou, L., Wadsworth, A., et al. (2020). Enhanced photocatalytic hydrogen evolution from organic semiconductor heterojunction nanoparticles. Nat. Mater. *19*, 559–565.
6. Wang, Z., Li, C., and Domen, K. (2019). Recent developments in heterogeneous photocatalysts for solar-driven overall water splitting. Chem. Soc. Rev. *48*, 2109–2125.
7. Zhang, N., Jalil, A., Wu, D., Chen, S., Liu, Y., Gao, C., Ye, W., Qi, Z., Ju, H., Wang, C., et al. (2018). Refining defect states in $W_{18}O_{49}$ by Mo doping: a strategy for tuning N_2 activation towards solar-driven nitrogen fixation. J. Am. Chem. Soc. *140*, 9434–9443.
8. Zhao, Y., Zhao, Y., Shi, R., Wang, B., Waterhouse, G.I.N., Wu, L., Tung, C., and Zhang, T. (2019). Tuning oxygen vacancies in ultrathin TiO_2 nanosheets to boost photocatalytic nitrogen fixation up to 700 nm. Adv. Mater. *31*, 1806482.
9. Takanabe, K. (2017). Photocatalytic water splitting: quantitative approaches toward photocatalyst by design. ACS Catal. *7*, 8006–8022.
10. Chen, X., Liu, L., Yu, P.Y., and Mao, S.S. (2011). Increasing solar absorption for photocatalysis with black hydrogenated titanium dioxide nanocrystals. Science *331*, 746–750.
11. Naldoni, A., Allieta, M., Santangelo, S., Marelli, M., Fabbri, F., Cappelli, S., Bianchi, C.L., Psaro, R., and Dal Santo, V. (2012). Effect of nature and location of defects on bandgap narrowing in black TiO2 nanoparticles. J. Am. Chem. Soc. *134*, 7600–7603.
12. Naldoni, A., Altomare, M., Zoppellaro, G., Liu, N., Kment, S., Zbořil, R., and Schmuki, P. (2019). Photocatalysis with reduced TiO_2: from black TiO_2 to cocatalyst-free hydrogen production. ACS Catal. *9*, 345–364.
13. Wang, X., Maeda, K., Thomas, A., Takanabe, K., Xin, G., Carlsson, J.M., Domen, K., and Antonietti, M. (2009). A metal-free polymeric photocatalyst for hydrogen production from water under visible light. Nat. Mater. *8*, 76–80.
14. Filippini, G., Longobardo, F., Forster, L., Criado, A., Carmine, G.D., Nasi, L., D'Agostino, C., Melchionna, M., Fornasiero, P., and Prato, M. (2020). Light-driven, heterogeneous organocatalysts for C–C bond formation toward valuable perfluoroalkylated intermediates. Sci. Adv. *6*, eabc9923.
15. Li, H., Chen, S., Shang, H., Wang, X., Yang, Z., Ai, Z., and Zhang, L. (2020). Surface hydrogen bond network spatially confined BiOCl oxygen vacancy for photocatalysis. Sci. Bull. *65*, 1916–1923.
16. Wu, Y.A., McNulty, I., Liu, C., Lau, K.C., Liu, Q., Paulikas, A.P., Sun, C.-J., Cai, Z., Guest, J.R., Ren, Y., et al. (2019). Facet-dependent active sites of a single Cu 2 O particle photocatalyst for CO 2 reduction to methanol. Nat. Energy *4*, 957–968.
17. Cargnello, M., Montini, T., Smolin, S.Y., Priebe, J.B., Jaén, J.J.D., Doan-Nguyen, V.V.T., McKay, I.S., Schwalbe, J.A., Pohl, M.-M., Gordon, T.R., et al. (2016). Engineering titania nanostructure to tune and improve its photocatalytic activity. PNAS *113*, 3966–3971.
18. Li, R., Zhang, F., Wang, D., Yang, J., Li, M., Zhu, J., Zhou, X., Han, H., and Li, C. (2013). Spatial separation of photogenerated electrons and holes among {010} and {110} crystal facets of $BiVO_4$. Nat. Commun. *4*, 1432. https://doi.org/10.1038/ncomms2401.
19. Chen, X., Shen, S., Guo, L., and Mao, S.S. (2010). Semiconductor-based photocatalytic hydrogen generation. Chem. Rev. *110*, 6503–6570.
20. Kamat, P.V., and Jin, S. (2018). Semiconductor photocatalysis: "*tell us the complete story!*". ACS Energy Lett. *3*, 622–623.
21. Schneider, J., and Bahnemann, D.W. (2013). Undesired role of sacrificial reagents in photocatalysis. J. Phys. Chem. Lett. *4*, 3479–3483.
22. Hainer, A.S., Hodgins, J.S., Sandre, V., Vallieres, M., Lanterna, A.E., and Scaiano, J.C. (2018). Photocatalytic hydrogen generation

using metal-decorated TiO_2: sacrificial donors vs true water splitting. ACS Energy Lett. *3*, 542–545.

23. Belhadj, H., Hamid, S., Robertson, P.K.J., and Bahnemann, D.W. (2017). Mechanisms of simultaneous hydrogen production and formaldehyde oxidation in H_2O and D_2O over platinized TiO_2. ACS Catal. *7*, 4753–4758.

24. Xu, C., Paone, E., Rodríguez-Padrón, D., Luque, R., and Mauriello, F. (2020). Recent catalytic routes for the preparation and the upgrading of biomass derived furfural and 5-hydroxymethylfurfural. Chem. Soc. Rev. *49*, 4273–4306.

25. Wu, X., Li, J., Xie, S., Duan, P., Zhang, H., Feng, J., Zhang, Q., Cheng, J., and Wang, Y. (2020). Selectivity control in photocatalytic valorization of biomass-derived platform compounds by surface engineering of titanium oxide. Chem *6*, 3038–3053.

26. Naldoni, A., Montini, T., Malara, F., Mróz, M.M., Beltram, A., Virgili, T., Boldrini, C.L., Marelli, M., Romero-Ocaña, I., Delgado, J.J., et al. (2017). Hot electron collection on brookite nanorods lateral facets for plasmon-enhanced water oxidation. ACS Catal. *7*, 1270–1278.

27. Di Valentin, C., Pacchioni, G., and Selloni, A. (2009). Reduced and n-type doped TiO_2: nature of Ti^{3+} species. J. Phys. Chem. C *113*, 20543–20552.

28. Wierzbicka, E., Altomare, M., Wu, M., Liu, N., Yokosawa, T., Fehn, D., Qin, S., Meyer, K., Unruh, T., Spiecker, E., et al. (2021). Reduced grey brookite for noble metal free photocatalytic H2 evolution. J. Mater. Chem. A *9*, 1168–1179.

29. Wang, H., Zhang, L., Chen, Z., Hu, J., Li, S., Wang, Z., Liu, J., and Wang, X. (2014). Semiconductor heterojunction photocatalysts: design, construction, and photocatalytic performances. Chem. Soc. Rev. *43*, 5234–5244.

30. Huang, H., Feng, J., Zhang, S., Zhang, H., Wang, X., Yu, T., Chen, C., Yi, Z., Ye, J., Li, Z., et al. (2020). Molecular-level understanding of the deactivation pathways during methanol photo-reforming on Pt-decorated TiO2. Appl. Catal. B Environ. *272*, 118980.

31. Bad'ura, Z., Naldoni, A., Qin, S., Bakandritsos, A., Kment, S., Schmuki, P., and Zoppellaro, G. (2021). Light-induced migration of spin defects in TiO2 nanosystems and their contribution to the H2 evolution catalysis from water. ChemSusChem *14*, 4408–4414.

32. Setvín, M., Aschauer, U., Scheiber, P., Li, Y.-F., Hou, W., Schmid, M., Selloni, A., and Diebold, U. (2013). Reaction of O_2 with subsurface oxygen vacancies on TiO_2 anatase (101). Science *341*, 988–991.

33. Naldoni, A., Riboni, F., Marelli, M., Bossola, F., Ulisse, G., Carlo, A.D., Píš, I., Nappini, S., Malvestuto, M., Dozzi, M.V., et al. (2016). Influence of TiO_2 electronic structure and strong metal–support interaction on plasmonic Au photocatalytic oxidations. Catal. Sci. Technol. *6*, 3220–3229.

34. Setvin, M., Shi, X., Hulva, J., Simschitz, T., Parkinson, G.S., Schmid, M., Di Valentin, C., Selloni, A., and Diebold, U. (2017). Methanol on anatase TiO_2 (101): mechanistic insights into photocatalysis. ACS Catal. *7*, 7081–7091.

35. Selcuk, S., and Selloni, A. (2016). Facet-dependent trapping and dynamics of excess electrons at anatase TiO2 surfaces and aqueous interfaces. Nat. Mater. *15*, 1107–1112.

36. Li, W.-K., Gong, X.-Q., Lu, G., and Selloni, A. (2008). Different reactivities of TiO_2 polymorphs: comparative DFT calculations of water and formic acid adsorption at anatase and brookite TiO_2 surfaces. J. Phys. Chem. C *112*, 6594–6596.

37. Naldoni, A., D'Arienzo, M., Altomare, M., Marelli, M., Scotti, R., Morazzoni, F., Selli, E., and Dal Santo, V. (2013). Pt and Au/TiO2 photocatalysts for methanol reforming: role of metal nanoparticles in tuning charge trapping properties and photoefficiency. Appl. Catal. B Environ. *130–131*, 239–248.

38. Setvin, M., Aschauer, U., Hulva, J., Simschitz, T., Daniel, B., Schmid, M., Selloni, A., and Diebold, U. (2016). Following the reduction of oxygen on TiO_2 anatase (101) step by step. J. Am. Chem. Soc. *138*, 9565–9571.